

# Resonance energies and linewidths of Rydberg excitons in Cu<sub>2</sub>O quantum wells

Niklas Scheuler,<sup>1</sup> Patric Rommel,<sup>1</sup> Jörg Main,<sup>1,\*</sup> and Pavel A. Belov<sup>2</sup>

<sup>1</sup>*Institut für Theoretische Physik 1, Universität Stuttgart, 70550 Stuttgart, Germany*

<sup>2</sup>*Institut für Physik, Universität Rostock, Albert-Einstein-Straße 23-24, 18059 Rostock, Germany*

(Dated: April 8, 2024)

Rydberg excitons are the solid-state analog of Rydberg atoms and can, e.g., for cuprous oxide, easily reach a large size in the region of  $\mu\text{m}$  for principal quantum numbers up to  $n = 25$ . The fabrication of quantum well-like structures in the crystal leads to quantum confinement effects and opens the possibility to study a crossover from three-dimensional to two-dimensional excitons. For small widths of the quantum well (QW) there are several well separated Rydberg series between various scattering thresholds leading to the occurrence of electron-hole resonances with finite lifetimes above the lowest threshold. By application of the stabilization method to the parametric dependencies of the real-valued eigenvalues of the original three-dimensional Schrödinger equation we calculate the resonance energies and linewidths for Rydberg excitons in QWs in regimes where a perturbative treatment is impossible. The positions and finite linewidths of resonances at energies above the third threshold are compared with the complex resonance energies obtained within the framework of the complex-coordinate-rotation technique. The excellent agreement between the results demonstrates the validity of both methods for intermediate sizes of the QW-like structures, and thus for arbitrary widths.

## I. INTRODUCTION

Excitons are electron-hole bound states in semiconductors [1]. The exciton states in bulk cuprous oxide (Cu<sub>2</sub>O) crystals are featured by relatively large binding energies as well as by unique radiative characteristics. The Rydberg states of excitons are, in turn, remarkable due to large spatial extent of the wave function and thus high sensitivity to the external fields [2] and surrounding quasiparticles [3]. In cuprous oxide, the typical size of the Rydberg exciton is in the order of  $\mu\text{m}$  for the principal quantum number of about  $n = 25$  [4–6]. The binding energies of the Rydberg states are less than 10 meV, though the tunability of the emitting light wavelengths makes them convenient for practical applications. This flexibility can be achieved by applying external fields [7, 8] or by fabrication of low-dimensional structures [9–12]. The latter can significantly change the energy spectrum of electron-hole pairs: in addition to features of the band structure, each quantum-confinement subband produces a proper Rydberg electron-hole series [11]. As a result, due to the Coulomb coupling of the upper subbands to the continuum of lower subbands, the electron-hole resonant states appear in the spectrum above the electron-hole scattering threshold.

Samples of cuprous oxide crystals of the size of order of  $\mu\text{m}$  are already produced, however, up to date, their quality allows one to observe only several lower exciton states [9]. Nevertheless, the technology is permanently developing and the low-dimensional samples of the size of hundreds nm with high radiative properties are expected to appear soon [10]. Very recently the fabrication of thin films with widths of about 20-30 nm has been reported

by Awal et al. [13]. In this sense, the ways to decrease the nonradiative broadening of the excited electron-hole states are especially important [14].

The simplest and most studied low-dimensional structure is a quantum well (QW) [15]. The exciton states in such a semiconductor structure have been actively studied for many years [16]. For example, there are recent studies of excitons in GaAs-, CdTe-, and GaN-based heterostructures [17–19]. However, the electron-hole resonances in such structures have been studied less intensively, mainly because of the square-unintegrable nature of the resonance wave function and resulting additional nonradiative linewidth broadening. Moreover, the results of earlier theoretical works on the broadening of excitons in GaAs-based QWs due to coupling to the continuum [20, 21] contradict more recent analytical estimates [22]. The first numerical investigations of electron-impurity and electron-hole resonant states using the finite-difference approach combined with the complex-coordinate-rotation method [23–25] have been done in Refs. [12, 26]. For the bulk Cu<sub>2</sub>O, there are also only a few recent studies of resonance linewidth broadenings [27, 28]. There is still no systematic study of the electron-hole resonances in QW-like structures, neither for the well-known GaAs-based structures, nor for the recently appearing cuprous oxide ones.

For the electron-hole pairs in GaAs-based structures, where the electron is much lighter than the hole, the problem can be reduced to a lower-dimensional model of an electron-impurity in a QW [12]. By contrast, comparable effective masses of the electrons and holes in cuprous oxide complicate the resonance calculation [6]. Furthermore, the perturbative solution of the Schrödinger equation for Rydberg excitons is only possible for the two limiting models of strong (narrow QW) and weak confinement (wide QWs, approaching the bulk crystal) [29]. However, for the model of intermediate QW

\* Email: main@itp1.uni-stuttgart.de

widths, a perturbative treatment is inapplicable and one has to solve the original three-dimensional equation numerically. The numerically obtained linewidth broadenings as well as reproduced absorption spectra based on mechanisms of exciton coupling to the continuum and to the phonon background can test the applicability of the Fano theory of resonances [30]. Moreover, the different parity of the subband eigenfunctions leads to a trivial example of the bound states in the continuum [31–33] and may further imply an existence of upper-lying states with negligible nonradiative broadening.

In this Paper, we calculate and identify the energies and the linewidths of electron-hole resonances in semiconductor heterostructures with intermediate QW widths for which the perturbative treatment is impossible. By our study, we show that the resonance parameters of Rydberg excitons in the continuum background can be readily obtained for arbitrary widths and relatively high energies. We use a hydrogenlike two-band model of the electron-hole pair in a QW structure [15] with the cuprous oxide material parameters [2], thus simulating the  $\text{Cu}_2\text{O}$  thin film sandwiched by vacuum or air. Note that the hydrogenlike model provides qualitatively good results to describe the exciton Rydberg series in the bulk up to small deviations caused by the band structure [4]. Here, we disregard features of the band structure, image charges [34] and finite potential in the substrate, as well as other effects which, for example, have been extensively employed to model the electron-hole bound states in GaAs-based QWs [11, 35]. Despite the above-mentioned assumptions, such a model leads to the three-dimensional Schrödinger equation [36], which produces the energy spectrum with quantum-confinement subbands and many different branches of the continua. Due to the Coulomb coupling of the upper quantum-confinement subbands to the continuum of lower ones, multiple electron-hole resonant states appear above the exciton states, namely above the scattering threshold  $E_{e1} + E_{h1}$ , where  $E_{e1/h1}$  is the lowest energy of the electron/hole in the QW. We show that the parity dependence of the eigenfunctions gives rise to the Rydberg series of bound states in the continuum [33].

To identify resonances above the lowest scattering threshold, we take advantage of the stabilization method [37–39] and compare the results with data obtained by the complex-coordinate-rotation technique. The complex-coordinate rotation is a general and well established method for the computation of resonances in open quantum systems. The method has already been used to investigate stationary systems, e.g., the resonant states of the hydrogen atom in external fields [40, 41], the helium atom [42], bulk and QW excitons [8, 26, 27], as well as time-dependent scattering problems [43, 44]. All above-cited theoretical works on semiconductor physics use this method as a reliable tool for obtaining the resonance energies and the linewidth broadenings. Although this approach is quite precise, it usually complicates the Hamiltonian by introducing the artificial complex-

rotational parameters, and, thus, leads to a solution of the non-Hermitian eigenvalue problem. An alternative technique which allows one to estimate the resonance parameters without making a complex rotation is the stabilization method. It has already been applied in a variety of works [45–49]. It solely implies rigid-wall boundary conditions at some distance from the interaction domain. Taking this distance as a parameter, the stabilization method is based on the observation of the parametric dependence of the energies of the discretized continuum. The avoided crossings of the discretized-continuum energy levels in the vicinity of the proper resonant energies allow one to estimate the linewidth broadenings of the resonances.

In our calculations within the stabilization method, the B-spline basis is employed to precisely compute the energy levels of the electron-hole pairs as well as their crossings and avoided crossings as a function of the QW width. The B-spline basis representation of the wave function allows for the fast and accurate solution of the three-dimensional Hermitian eigenvalue problem. Besides the high accuracy of the results produced by the high-order B-spline calculations, the minimal support of the B-splines leads to minimal overlaps and thus to the band structure of the matrices of the corresponding generalized eigenvalue problem. Moreover, the obtained parametric dependence of the energies on the QW width makes it possible to accurately determine the linewidths of the electron-hole resonant states by the stabilization method. Comparison of the results computed by the stabilization method with ones obtained from the non-Hermitian eigenvalue problem in the framework of the complex-coordinate-rotation technique shows an excellent agreement. It justifies the validity of both methods for the intermediate sizes of the QW-like structures, and thus for arbitrary widths. This also paves the way for more detailed calculations and facilitates further analysis of the experimental data [9].

## II. THEORY AND METHODS

We now present and discuss the Hamiltonian of the exciton in a QW, its energy spectrum, the B-spline basis for the efficient numerical solution of the Schrödinger equation, and two different methods for the computation of resonance energies and linewidths.

### A. Excitons in cuprous oxide QWs

The two-band model for the electron-hole pair in a cuprous oxide QW is given as

$$H = E_g - \frac{\hbar^2}{2m_e} \Delta_e - \frac{\hbar^2}{2m_h} \Delta_h - \frac{1}{4\pi\epsilon_0\epsilon} \frac{e^2}{|\mathbf{r}_e - \mathbf{r}_h|} + V_e(z_e) + V_h(z_h), \quad (1)$$

with

$$V_{e,h}(z_{e,h}) = \begin{cases} 0, & \text{if } |z_{e,h}| < L/2 \\ \infty, & \text{if } |z_{e,h}| > L/2 \end{cases}. \quad (2)$$

Here,  $m_e = 0.99 m_0$  and  $m_h = 0.69 m_0$  are the effective masses of the electron (e) and the hole (h), respectively,  $E_g = 2.17208 \text{ eV}$  is the band gap energy,  $e$  is the electron charge,  $\varepsilon_0$  is the electric constant,  $\varepsilon = 7.5$  is the dielectric constant, and  $L$  is the width of the QW. The infinite potential in the substrate is an approximation, however, such an infinite-barrier potential can be a reasonable model for a thin cuprous oxide film surrounded by vacuum or air [10]. We separate the center-of-mass motion in the QW plane and use polar coordinates  $(\rho, \phi)$  to describe the relative motion. The rotational symmetry around the  $z$ -axis implies the conservation of the  $z$  component of the angular momentum with quantum number  $m$ , and we arrive at the three-dimensional equation

$$H\Psi(\rho, z_e, z_h) = E\Psi(\rho, z_e, z_h), \quad (3)$$

with the Hamiltonian

$$H = E_g - \frac{\hbar^2}{2\mu} \left( \frac{\partial^2}{\partial \rho^2} + \frac{1}{\rho} \frac{\partial}{\partial \rho} - \frac{m^2}{\rho^2} \right) - \frac{\hbar^2}{2m_e} \frac{\partial^2}{\partial z_e^2} - \frac{\hbar^2}{2m_h} \frac{\partial^2}{\partial z_h^2} - \frac{1}{4\pi\varepsilon_0\varepsilon} \frac{e^2}{\sqrt{\rho^2 + (z_e - z_h)^2}} + V_e(z_e) + V_h(z_h). \quad (4)$$

Here,  $\mu$  is the reduced mass, and the angular momentum quantum number  $m = 0, \pm 1, \pm 2, \dots$  is a good quantum number. Besides  $m$  there is one additional exact quantum number, i.e., the parity  $\pi_z = \pi_{z_e} \pi_{z_h} = \pm 1$ , which is related to the simultaneous exchange of  $z_e \rightarrow -z_e$  and  $z_h \rightarrow -z_h$ .

## B. Energy spectrum

The Hamiltonian (4) defines the energy spectrum of the electron-hole bound states and resonances in the QW. The bound states correspond to the square-integrable solutions of the Schrödinger equation, whereas the resonances are associated to the square-unintegrable ones. A resonant state can be considered as a quasi-bound state with a finite lifetime due to an exponential decay, which can be described as  $\Psi(t) = \exp(-iEt/\hbar)\Psi(0)$  with a complex energy [50, 51]

$$E = E_{\text{res}} - i\frac{\Gamma}{2}, \quad (5)$$

where  $E_{\text{res}}$  is the resonance position and  $\Gamma > 0$  is the linewidth. It means that the resonance wave function does not exponentially decrease as  $\rho \rightarrow \infty$ , and thus these states cannot be determined in terms of the Hermitian quantum theory [25].

Each disjoint subsystem (the electron or the hole in the QW) of the Hamiltonian (4) produces a series

of quantum-confinement energies  $E_{ei/hj}(L)$  with  $i, j = 1, \dots, \infty$ . Moreover, the Coulomb attraction leads to Rydberg energy series below each value of the sum

$$E_{i,j}(L) \equiv E_{ei}(L) + E_{hj}(L) = \frac{\hbar^2(i\pi)^2}{2m_e L^2} + \frac{\hbar^2(j\pi)^2}{2m_h L^2}. \quad (6)$$

For a particular  $L$ , each such a value appears to be a scattering threshold, giving rise to a certain branch of the continuum. In case of strong confinement, exciton states and electron-hole resonances with the respective parity are located below the thresholds. In this limit, the exciton wave function is factorized  $\Psi_{nij}(\rho, z_e, z_h) = R_n^{2D}(\rho)\psi_{ei}(z_e)\psi_{hj}(z_h)$ , where  $R_n^{2D}(\rho)$ ,  $n = 1, \dots, \infty$  are the 2D Coulomb radial eigenfunctions and  $\psi_{ei/hj}(z_{e/h})$  are the quantum-confinement eigenmodes [11]. The quantum numbers  $i, j$  and the principal quantum number  $n$  are the good ones. Note that the Rydberg formula reads  $E_n = -E_{\text{Ryd}}/(n - 1/2)^2$  in two dimensions. For weaker confinement, the wave function is no longer factorized and the quantum numbers of the states can only be associated approximately. The resonances with different parity can strongly overlap. Below the lowest threshold,  $E_{1,1} = E_{e1} + E_{h1}$ , there are the bound states. Above this threshold the resonant states appear in the continuum background [11], except for odd parity bound states, which, for  $m_e > m_h$ , appear up to the first odd parity threshold  $E_{2,1} = E_{e2} + E_{h1}$ . The decay of these odd parity bound states in the continuum background of the even parity states is forbidden, i.e., the widths are exactly  $\Gamma = 0$  [33].

The energies of the states defined by Eq. (4) can be obtained analytically only in the limiting cases of strong confinement or weak confinement, when the Coulomb potential or the effect of QW barriers can, respectively, be treated as a small perturbation [29]. For arbitrary QW width  $L$ , Eq. (3) can only be solved numerically [36]. Moreover, the efficient numerical approach allows one to apply the stabilization method [37–39] or the complex-coordinate-rotation method [23, 24] to go beyond Hermitian physics and to precisely estimate not only the resonance energies, but also the linewidths.

## C. Computation of the energy spectrum

The Schrödinger equation (3) was already treated numerically using the finite-difference and basis-expansion approaches [36, 52, 53]. These methods are appropriate for the bound state calculations of lower exciton states. However, for a precise determination of the Rydberg energies or resonances associated to upper scattering thresholds one has to use fine grids over a broad calculation domain or take many basis functions. Moreover, the integration of the quantum-confinement basis functions having nonzero support over the whole domain is usually also quite time-consuming.

To overcome these computational issues and accurately estimate the resonance linewidths, we use the expansion

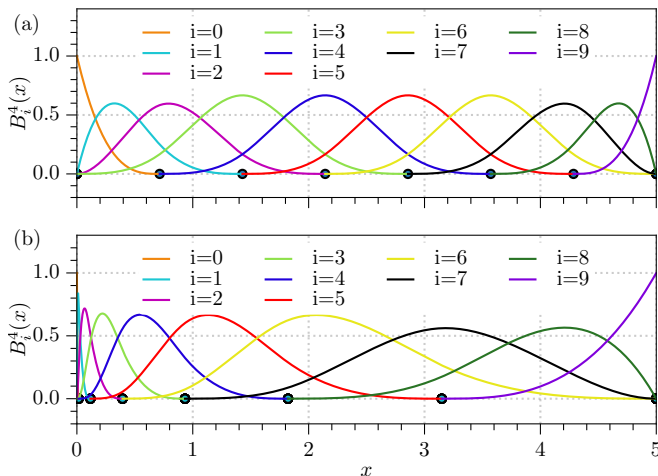


FIG. 1. B-spline functions with (a) equidistant and (b) non-equidistant spacing of knots and additional ghost knots at the boundaries. When the first and last B-splines are removed, the functions satisfy vanishing boundary conditions.

of the wave function over a basis of B-splines [54]. The B-splines  $B_i^k(x)$ ,  $i = 1, \dots, n$  are piecewise polynomials of degree  $k - 1$ , which can be generated by recursive formulas with knots  $t_i$  [55]. For example, for  $k = 1$  the B-splines are piecewise-constant, for  $k = 2$  they are piecewise-linear functions. Some B-splines with  $k = 4$  and different knots are illustrated in Fig. 1. Three important properties of B-splines should be mentioned. Firstly, the B-spline of order  $k$  on a grid of equidistant knots approximates an analytical function with accuracy of about  $h^k$ , where  $h$  is the step size of the grid. Thus, high-order B-splines can give a precise solution even with a relatively small number of knots. Secondly, one can choose the knots non-equidistantly and add ghost knots at the boundaries in such a way as to have two B-splines equal to 1 in the two boundary points, while all other B-splines vanish in these points (see Fig. 1). Then, for example, zero boundary conditions can be easily implemented by removing the first and the last B-splines from the basis. Thirdly, the B-splines are nonorthogonal functions, and thus Eq. (3) turns into a generalized eigenvalue problem

$$\sum_n H_{mn} c_n = E \sum_n O_{mn} c_n, \quad (7)$$

with  $O_{mn}$  the overlap matrix between the basis functions. However, the B-spline functions have minimal support, i.e., each B-spline  $B_i^k(x) = 0$  for  $x \notin [t_i, t_{i+k}]$ , which significantly reduces the number of integrations to calculate matrix elements. This leads to the band structure of matrices or to sparse matrices of the generalized eigenvalue problem (7) for one- or higher-dimensional problems, respectively.

When applying B-splines to the QW problem with the Hamiltonian (4) it should be noted that the QW potentials imply zero boundary conditions at  $z_{e,h} = \pm L/2$ . This can be achieved by a proper choice of the B-spline

basis. The boundary conditions in the  $\rho$ -direction are less obvious. The wave function  $\psi$  is finite but not necessarily zero at  $\rho = 0$ . To implement a zero boundary condition at  $\rho = 0$ , we use the substitution  $\psi = \chi/\sqrt{\rho}$ . As a result of the substitution, the B-spline expansion of  $\chi$  is employed with the Hamiltonian

$$H = E_g - \frac{\hbar^2}{2\mu} \left( \frac{\partial^2}{\partial \rho^2} - \frac{m^2 - 1/4}{\rho^2} \right) - \frac{\hbar^2}{2m_e} \frac{\partial^2}{\partial z_e^2} - \frac{\hbar^2}{2m_h} \frac{\partial^2}{\partial z_h^2} - \frac{1}{4\pi\epsilon_0\epsilon} \frac{e^2}{\sqrt{\rho^2 + (z_e - z_h)^2}} \quad (8)$$

and the zero boundary conditions at  $z_{e,h} = \pm L/2$ . Note that now the QW potentials in Eq. (4) are ignored in Eq. (8). We artificially introduce an additional zero boundary condition at a large value  $\rho = \rho_{\max}$ , thus making a box-like geometry in this direction. If the parameter  $\rho_{\max}$  is sufficiently large, the spectrum of bound states below the scattering threshold is well approximated. However, without application of further methods we obtain a discretized continuum instead of the true resonances above the thresholds.

In our calculations, we use the expansion

$$\chi(z_e, z_h, \rho) \approx \sum_{l=1}^{\tilde{N}_{z_e}} \sum_{m=1}^{\tilde{N}_{z_e}} \sum_{n=1}^{\tilde{N}_{z_h}} c_{lmn} B_{l+1}^k(z_e) B_{m+1}^k(z_h) B_{n+1}^k(\rho) \quad (9)$$

with B-splines of order  $k = 5$  and equidistant knots in the  $z$ -directions, but non-equidistant knots in the  $\rho$ -direction similarly as illustrated in Fig. 1(b). In Eq. (9)  $\tilde{N}_q = N_q + k - 4$ , where  $N_q$  is the number of physical knots in the  $q$  direction. For all directions,  $k - 1$  ghost knots were inserted at the boundaries, to be able to define at least  $k - 1$  B-splines at each interval. For the  $\rho$ -direction the  $i$ -th knot between the ghost knots is calculated via

$$\rho_{i+k-1} = \left( \frac{i - k}{N_\rho - 1} \right)^3 \rho_{\max}. \quad (10)$$

We used 30 physical knots for the  $\rho$ -direction and 22 knots for each of two  $z$ -coordinates. The matrix elements were calculated numerically by application of a 15 point Gauss-Kronrod formula [56]. To speed up calculations, only matrix elements that do not vanish due to the finite support of the B-splines are calculated. The generalized eigenvalue problem (7) with symmetric, sparse, and banded matrices, was solved by LAPACK routines [57].

#### D. Stabilization method

The stabilization method allows for the calculation of the complex resonance energies directly from the Hermitian eigenvalue problem with the Hamiltonian (8). The idea is to analyze the real-valued spectrum of the Hamiltonian (8) as a function of the box size parameter  $\rho_{\max}$ . This yields the so-called stabilization diagram, i.e., a

graph containing curves  $E_j(\rho_{\max})$  with  $j$  counting the (real-valued) eigenvalues. For sufficiently large values of  $\rho_{\max}$ , the energies belonging to resonant states stabilize, i.e., they are almost independent of  $\rho_{\max}$  with the exception of regions close to avoided crossings with energies of the discretized continuum in the box. The density of states  $\varrho(E)$  is then extracted from the slopes of the curves in the stabilization diagram as [38, 39]

$$\varrho(E) = \frac{1}{\Delta\rho_{\max}} \sum_j \left| \frac{dE_j(\rho'_{\max})}{d\rho'_{\max}} \right|_{E_j(\rho'_{\max})=E}^{-1}. \quad (11)$$

In open systems the density of states is typically given as a superposition of Lorentzians, and therefore, in the final step, the energy positions  $E_{\text{res}}$  and widths  $\Gamma$  of isolated resonances can be extracted from the density profile (11) by fitting

$$\varrho(E) \simeq \pi^{-1} \frac{\Gamma/2}{(E_{\text{res}} - E)^2 + \Gamma^2/4}. \quad (12)$$

### E. Complex-coordinate-rotation method

The basic idea of the complex-coordinate-rotation method is to do the transformation  $r \rightarrow r e^{i\theta}$  with  $\theta > 0$ , which yields a non-Hermitian Hamiltonian. The energies of the bound states are invariant under this transformation, while the energies of the continuum states are rotated into the lower half of the complex plane by the angle  $2\theta$ . Most interesting for our application is the impact on resonant states. The complex eigenvalues, corresponding to the resonant states, are located in the sector of the angle  $2\theta$  between the lowest rotated branch of the continuum and the real axis. They are independent or only weakly dependent of the angle of the rotation if the angle is large enough to contain the unknown eigenvalue.

For our problem the complex-coordinate rotation is restricted to the  $\rho$ -coordinate because the system is open only in this direction. The boundary conditions in the  $z$ -directions must not be changed by a complex rotation. The substitution  $\rho \rightarrow \rho e^{i\theta}$  transforms the Hamiltonian (8) to

$$H = E_g - e^{-2i\theta} \frac{\hbar^2}{2\mu} \left( \frac{\partial^2}{\partial \rho^2} - \frac{m^2 - 1/4}{\rho^2} \right) - \frac{\hbar^2}{2m_e} \frac{\partial^2}{\partial z_e^2} - \frac{\hbar^2}{2m_h} \frac{\partial^2}{\partial z_h^2} - \frac{1}{4\pi\epsilon_0\epsilon} \frac{e^2}{\sqrt{e^{2i\theta}\rho^2 + (z_e - z_h)^2}}. \quad (13)$$

This leads to the generalized eigenvalue problem (7) with non-Hermitian, complex symmetric matrices, which is efficiently solved by using the ARPACK package [58]. Note that the angle  $\theta$  must be chosen appropriately to obtain convergence of the results [51].

## III. RESULTS AND DISCUSSION

In Fig. 2(a) we present the real-valued energy eigenvalues for excitons in cuprous oxide QWs described by the Hermitian Hamiltonian (8) as a function of the width  $L$  of the QW. The computations have been performed for angular quantum number  $m = 1$  and for a fixed value of the box size parameter  $\rho_{\max} = 500$  nm. The first four thresholds  $E_{i,j}(L) = E_{ei}(L) + E_{hj}(L)$  [see Eq. (6)] are marked as colored lines. For a better visualization of the bound states the energy of the first threshold  $E_{1,1}$  has been subtracted. As explained above, only the bound states, i.e., the even parity states below threshold  $E_{1,1}$  and the odd parity states below the threshold  $E_{2,1}$  are converged states, which do not depend on the box size  $\rho_{\max}$ . The energy levels of the bound states exhibit the crossover from the model of the narrow QW (2D Coulomb potential) at low values of  $L$  to the model of the bulk crystal (3D Coulomb potential) at large  $L$  [11]. When the QW width is increased, the thresholds gradually descent to the lowest one. As a result, the states associated to upper thresholds get down below the lowest threshold and the number of bound states increases. In contrast to the limiting cases, for intermediate QW widths the principal quantum number  $n$  and the quantum-confinement ones  $i$  and  $j$  lose their status as good quantum numbers. However, it remains possible to assign approximate quantum numbers to most of the states. A detailed discussion of the bound states is given in Ref. [29]. All other states above the respective thresholds are, in principle, the unphysical discretized continuum states. The continuum region becomes more pronounced in Fig. 2(b), where we show the same states as in (a) but with respect to the threshold  $E_{2,2}$ . We highlight five of the discretized continuum states with approximate principal quantum numbers  $n = 3$  to 6 (belonging to different thresholds) at QW width  $L = 8$  nm by red markers. Such a QW width corresponds to the crossover region of QW widths, when none of the limiting models is applicable. On the one hand, this region is interesting due to the fact that Rydberg excitons with principal quantum numbers  $n \sim 3$  to 6 are significantly disturbed compared to bulk excitons. On the other hand, the Rydberg series related to the different channels do not overlap too strongly to complicate the analysis of spectra and the discussion. A recent study demonstrated the feasibility of fabricating nanostructures composed of  $\text{Cu}_2\text{O}$  at this scale [13]. Since these states are in the continuum, the related resonances have nonzero linewidths. Note from Fig. 2(b) that there is an additional discretized continuum state a little bit below of the second marked resonance state at  $L = 8$  nm. It originates purely from the rigid-wall boundary conditions, therefore we disregard this unphysical eigenvalue.

Although Fig. 2 provides a massive amount of information on the dependence of Rydberg energies on the QW width, it is not sufficient to determine the resonance linewidths. To this end, we employed the two above-mentioned methods. As a first technique, we ap-

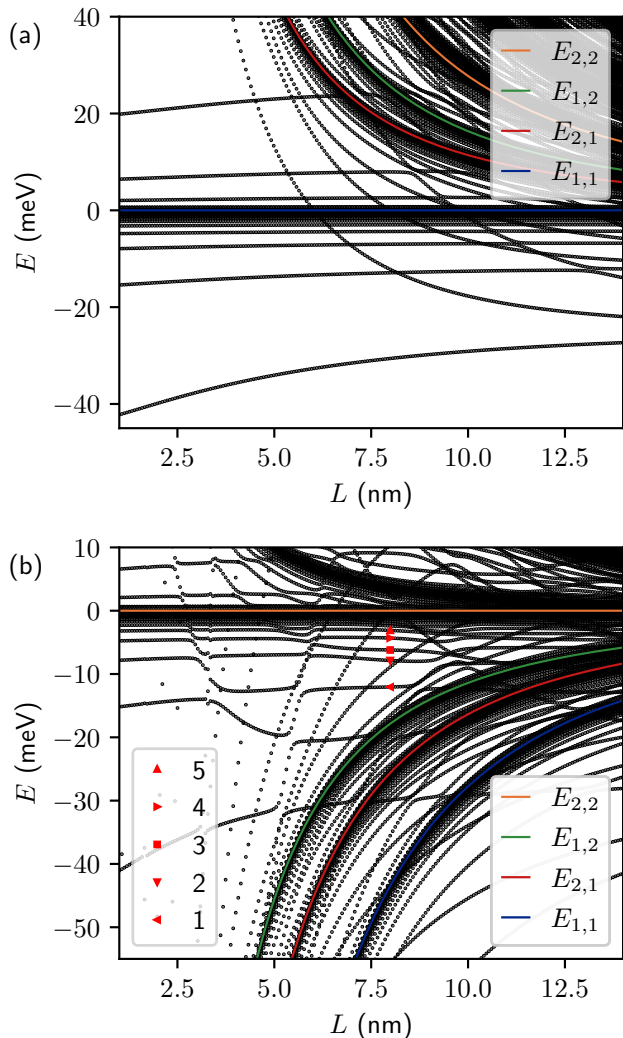


FIG. 2. Spectrum of the Hamiltonian (8) with respect to (a) the threshold  $E_{1,1}(L)$  and (b) the threshold  $E_{2,2}(L)$  as a function of the QW width. Note that the energy scales differ from the energy scale in Fig. 4, where absolute values are given. The angular quantum number is  $m = 1$ , and the box size parameter is  $\rho_{\max} = 500$  nm. The five resonant states at  $L = 8$  nm, which are investigated with the stabilization method and the complex-coordinate-rotation method are highlighted in (b) by red markers.

ply the stabilization method to obtain the energies and linewidths of these resonances from the real-valued numerical data of energy levels in the continuum region. To this aim, the stabilization diagram shown in Fig. 3(a) has been calculated in the region from  $\rho_{\max} = 300$  nm to  $\rho_{\max} = 700$  nm. Clearly visible is the stabilization of several resonant states as segments of approximately vertical lines separated by avoided crossings. For five selected resonant states, lower and upper segments, labeled as ‘a’ and ‘b’ in what follows, are highlighted by solid and dashed colored lines, respectively. If these resonant states were bound states they would not depend

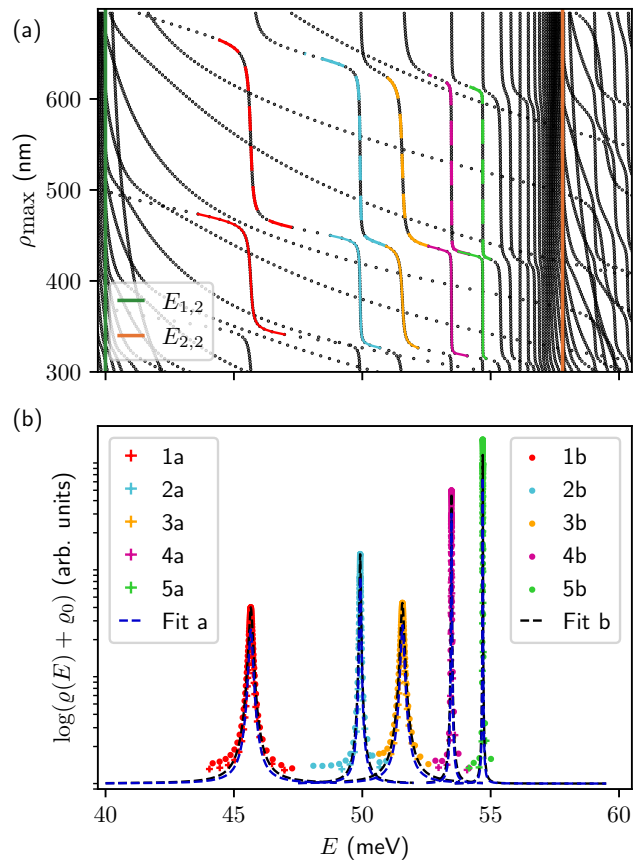


FIG. 3. Application of the stabilization method for the QW width  $L = 8$  nm and  $m = 1$  for the resonances highlighted in Fig. 2(b). Note that here we show absolute resonance energies, which differ from the values in Fig. 2(b), where the threshold energy  $E_{2,2}(L)$  has been subtracted. (a) Stabilization diagram in the region from  $\rho_{\max} = 300$  nm to  $\rho_{\max} = 700$  nm. Segments belonging to the studied resonant states are highlighted by the colored solid and dashed lines. They refer to the states 1-5 in Fig. 2(b). (b) Logarithm of the density of states as a function of energy  $E$ . Colored peaks marked as ‘a’ and ‘b’ are obtained from the solid and dashed segments in (a), respectively. For a better visualization,  $\varrho(E)$  is shifted upwards by a small value  $\varrho_0$ , so that  $\log(\varrho)$  is bounded from below by a constant value. The crosses and the dots represent  $\varrho(E)$  calculated by Eq. (11). The dashed lines represent the fits to the Lorentzian shape given in Eq. (12).

on the box-size parameter  $\rho_{\max}$  and thus appear, without undergoing any avoided crossings, as exactly vertical lines in the stabilization diagram. The deviations from exact vertical lines and in particular the avoided crossings with some of the  $\rho_{\max}$ -dependent continuum states indicate the coupling to the continuum, i.e., the stabilized states are resonances with finite lifetimes. Their slopes and avoided crossings allow for the computation of their line shapes via Eq. (11). The density of states resulting from the application of Eq. (11) to the highlighted segments in Fig. 3(a) is presented in Fig. 3(b) and



TABLE I. Complex resonance energies (in meV) of the five selected states with approximate principal quantum numbers  $n = 3$  to 6, which refer to the thresholds  $E_{2,2}$  and  $E_{3,1}$  obtained with the stabilization method and the complex-coordinate-rotation method. The assigned approximate quantum numbers of the QW eigenstates and the principal quantum numbers  $n$  are listed in the first three columns. The linewidths of the resonances are given as  $\Gamma = -2 \text{Im } E$ . For the analyzed states, the stabilization method was applied to two different segments highlighted by solid and dashed colored curves in Fig. 3 (see text), resulting in the values denoted by indices ‘a’ and ‘b’, respectively.

$i$	$j$	$n$	segment	Stabilization method		Complex rotation	
				Re $E$	Im $E$	Re $E$	Im $E$
2	2	3	1a	45.6577	-0.0815	45.6607	-0.0798
			1b	45.6547	-0.0812		
2	2	4	2a	49.9181	-0.0242	49.9189	-0.0239
			2b	49.9164	-0.0229		
3	1	3	3a	51.5645	-0.0670	51.5665	-0.0691
			3b	51.5613	-0.0705		
2	2	5	4a	53.4736	-0.0060	53.4738	-0.0060
			4b	53.4738	-0.0062		
2	2	6	5a	54.6914	-0.0020	54.6915	-0.0020
			5b	54.6914	-0.0019		

exhibits peaks with various widths and heights at the resonance positions. These peaks are fitted by Eq. (12) to a Lorentzian shape to obtain the resonance positions  $E_{\text{res}}$  and linewidths  $\Gamma$ . The corresponding values obtained by the stabilization method are given in columns 5 and 6 of Table I. Note that the densities of states as well as Lorentzian fits labeled as ‘a’ and ‘b’ are obtained respectively from the lower and upper series of highlighted segments in the stabilization diagram [Fig. 3(a)]. Both fits for a given resonance and, as a result, the corresponding complex energies in Table I are nearly identical. This indicates that the sum in Eq. (11) is well approximated by the first terms.

We now apply a second technique, and compare the data obtained by the stabilization method with the results of the complex-coordinate-rotation method, i.e. with the eigenvalues of the non-Hermitian Hamiltonian (13). In our calculations, the angle of the coordinate rotation is  $\theta = 0.1$ . We note that the results presented in Fig. 4 and Table I are fully converged to numerical accuracy for rotation angles in the region  $\theta \sim 0.1 - 0.2$ . The resonance positions in the complex energy plane for the QW width  $L = 8$  nm and the angular momentum quantum number  $m = 1$  are shown in Fig. 4. The Rydberg bound states are located on the real axis with  $\text{Im } E = 0$ . The scattering thresholds  $E_{i,j}$  given in Eq. (6) are marked by colored vertical lines. Clearly visible are the accumulation of even parity bound states with  $\pi_z = +1$  below the first scattering threshold  $E_{1,1}$ , the accumulation of odd parity bound states with  $\pi_z = -1$  below the second (odd parity) scattering threshold  $E_{2,1}$ , and the discretized continuum states related to the various scatter-

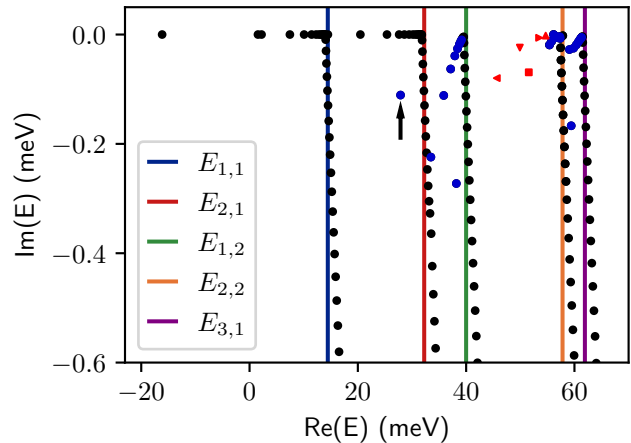


FIG. 4. Eigenvalues of the complex-coordinate-rotated Hamiltonian (13) for the QW width  $L = 8$  nm and the angular momentum quantum number  $m = 1$ . Note that the resonance positions are shifted compared to Fig. 2(b), since there no threshold energy has been subtracted. The first five threshold energies  $E_{i,j}$  are shown as colored lines. The five selected resonances, which have been analyzed by application of the stabilization method are marked by red markers, while all other resonances are represented by blue dots. The even parity resonance below the threshold  $E_{2,1}$  is marked by an arrow.

ing thresholds, which are rotated into the lower half of the complex plane by the angle  $2\theta$ . Although the Rydberg series of the odd parity bound states is in the continuum background of the even parity states, the states of different parity are uncoupled. As a result, the calculated  $\text{Im } E$  of these odd parity bound states are zero to numerical precision. The remaining states are the resonance states with finite lifetimes, i.e.,  $\text{Im } E < 0$ ; they are denoted by colored markers. The five selected resonances, which have already been studied by application of the stabilization method, are marked by red markers. Their resonance energies are listed in the two last columns of Table I. One can see an excellent agreement between the results of the stabilization method and the complex-coordinate-rotation method.

When the QW width is small, the quantum-confinement thresholds are well separated. When the QW width is increased, the thresholds gradually descent to the lowest one. As a result, the resonances of the current threshold get down below the adjacent lower thresholds. For QW width  $L = 8$  nm, such a penetration is shown by a small number of resonances, that simplifies the current analysis. For example, this can clearly be seen in Fig. 4 by the even parity resonance with the distinct complex eigenvalue  $E = (27.8840 - i0.1107)$  meV marked by the arrow, which is below the  $E_{2,1}$  scattering threshold.

#### IV. CONCLUSIONS

In QWs, multiple Rydberg series of electron-hole resonances appear above the lowest scattering threshold due to the Coulomb coupling of the upper quantum-confinement subbands to the continuum of lower ones. These Rydberg series are well separated in case of the strong confinement, therefore the approximate perturbative treatment of the scattering problem is possible [22]. For arbitrary QW widths, in particular, for intermediate thicknesses, a precise determination of the resonance parameters can only be done using a numerical solution. In our Paper, we identified the Rydberg series of electron-hole resonances in cuprous oxide QW and accurately calculated their energies and linewidths for the thickness, for which the resonances of different thresholds do not significantly overlap. To this end, the efficient numerical method based on the expansion of the wave function of the original three-dimensional Schrödinger equation over a basis of B-splines was developed. It made it possible to study the dependence of the numerical solution on the size of the calculation domain in the broad range of the parameter variance. The lifetimes of the resonant states were calculated using the stabilization method, allowing to derive the density of states and the resonant parameters from the solution of the real-valued eigenvalue problem. The obtained numerical results are compared with the data calculated by the complex-coordinate-rotation method. The agreement of the results allows us to demonstrate the applicability of both methods to study electron-hole resonances in QWs

of arbitrary widths. In particular, we obtained that independent of the QW thickness, the two lowest Rydberg series of states, below the second threshold, are bound states. The first series is associated to the even parity bound states and the second one is associated to odd parity bound states in the even parity continuum. As a result, for the strong confinement, the nonvanishing broadening is proper to the upper-lying resonance states. However, with the crossover to the weak confinement, the partial overlap of the Rydberg series is increased, resonances get down below, and the analysis of the results becomes more complicated.

The presented methods to study the selected electron-hole resonances open up the opportunity to investigate other features of resonant states, e.g., the threshold effects of resonances by varying the QW width. Moreover, taking into account the full valence band structure of cuprous oxide and using the eigenstates for the simulation of absorption spectra will allow for detailed comparisons of our theoretical results with future experimental measurements.

#### ACKNOWLEDGMENTS

This work was supported by Deutsche Forschungsgemeinschaft (DFG) through Grant No. MA 1639/16-1. P.A.B. acknowledges financial support from Deutscher Akademischer Austauschdienst (DAAD) and the DFG Priority Programme 1929 “*Giant interactions in Rydberg Systems*” (GiRyd), Grant No. SCHE 612/4-2. We thank Stefan Scheel for fruitful discussions.

- 
- [1] E. Rashba and M. Sturge, eds., *Excitons: Selected Chapters* (North-Holland Amsterdam, 1982).
- [2] F. Schweiner, J. Main, G. Wunner, M. Freitag, J. Heckötter, C. Uihlein, M. Aßmann, D. Fröhlich, and M. Bayer, Magnetoexcitons in cuprous oxide, *Phys. Rev. B* **95**, 035202 (2017).
- [3] D. Semkat, H. Fehske, and H. Stolz, Influence of electron-hole plasma on Rydberg excitons in cuprous oxide, *Phys. Rev. B* **100**, 155204 (2019).
- [4] T. Kazimierczuk, D. Fröhlich, S. Scheel, H. Stolz, and M. Bayer, Giant Rydberg excitons in the copper oxide Cu<sub>2</sub>O, *Nature* **514**, 343 (2014).
- [5] J. Thewes, J. Heckötter, T. Kazimierczuk, M. Aßmann, D. Fröhlich, M. Bayer, M. A. Semina, and M. M. Glazov, Observation of high angular momentum excitons in cuprous oxide, *Phys. Rev. Lett.* **115**, 027402 (2015).
- [6] F. Schweiner, J. Main, M. Feldmaier, G. Wunner, and C. Uihlein, Impact of the valence band structure of Cu<sub>2</sub>O on excitonic spectra, *Phys. Rev. B* **93**, 195203 (2016).
- [7] A. Farenbruch, D. Fröhlich, D. R. Yakovlev, and M. Bayer, Rydberg series of dark excitons in Cu<sub>2</sub>O, *Phys. Rev. Lett.* **125**, 207402 (2020).
- [8] P. Zielinski, P. Rommel, F. Schweiner, and J. Main, Rydberg excitons in electric and magnetic fields obtained with the complex-coordinate-rotation method, *Journal of Physics B: Atomic, Molecular and Optical Physics* **53**, 054004 (2020).
- [9] M. Takahata, K. Tanaka, and N. Naka, Nonlocal optical response of weakly confined excitons in Cu<sub>2</sub>O mesoscopic films, *Phys. Rev. B* **97**, 205305 (2018).
- [10] A. Konzelmann, B. Frank, and H. Giessen, Quantum confined Rydberg excitons in reduced dimensions, *Journal of Physics B: Atomic, Molecular and Optical Physics* **53**, 024001 (2019).
- [11] P. A. Belov, Energy spectrum of excitons in square quantum wells, *Physica E: Low-dimensional Systems and Nanostructures* **112**, 96 (2019).
- [12] P. A. Belov, Linewidths and energy shifts of electron-impurity resonant states in quantum wells with infinite barriers, *Phys. Rev. B* **105**, 155417 (2022).
- [13] R. Awal, N. Y. Tanisa, M. A. Rahman, and S. Ahmed, Preparation of nanostructured cuprous oxide (Cu<sub>2</sub>O) absorber layer for photovoltaic application, *Micro & Nano Letters* **19**, e12188 (2024).
- [14] S. V. Poltavtsev, Y. P. Efimov, Y. K. Dolgikh, S. A. Eliseev, V. V. Petrov, and V. V. Ovsyankin, Extremely low inhomogeneous broadening of exciton lines in shallow (In,Ga)As/GaAs quantum wells, *Solid State Communi-*



- cations **199**, 47 (2014).
- [15] E. Ivchenko, *Optical Spectroscopy of Semiconductor Nanostructures* (Alpha Science, 2005).
- [16] C. Klingshirn, *Semiconductor Optics*, Advanced Texts in Physics (Springer, Berlin, Heidelberg, 2007).
- [17] E. Laird, F. M. Marchetti, D. K. Efimkin, M. M. Parish, and J. Levinsen, Rydberg exciton-polaritons in a magnetic field, *Phys. Rev. B* **106**, 125407 (2022).
- [18] L. V. Kotova, A. V. Platonov, R. André, H. Mariette, and V. P. Kochereshko, Interface birefringence in asymmetric CdTe/CdZnTe quantum wells, *Phys. Rev. B* **107**, 235302 (2023).
- [19] F. Chiaruttini, T. Guillet, C. Brimont, D. Scalbert, S. Cronenberger, B. Jouault, P. Lefebvre, B. Damilano, and M. Vladimirova, Complexity of the dipolar exciton Mott transition in GaN/(AlGa)N nanostructures, *Phys. Rev. B* **103**, 045308 (2021).
- [20] D. A. Broido, E. S. Koteles, C. Jagannath, and J. Y. Chi, Resonance broadening of the light-hole exciton in GaAs/Al<sub>x</sub>Ga<sub>1-x</sub>As quantum wells, *Phys. Rev. B* **37**, 2725 (1988).
- [21] A. Pasquarello and L. C. Andreani, Variational calculation of fano linewidth: Application to excitons in quantum wells, *Phys. Rev. B* **44**, 3162 (1991).
- [22] B. S. Monozon and P. Schmelcher, Resonant impurity and exciton states in a narrow quantum well, *Phys. Rev. B* **71**, 085302 (2005).
- [23] W. P. Reinhardt, Complex coordinates in the theory of atomic and molecular structure and dynamics, *Annual Review of Physical Chemistry* **33**, 223 (1982).
- [24] Y. K. Ho, The method of complex coordinate rotation and its applications to atomic collision processes, *Phys. Rep.* **99**, 1 (1983).
- [25] N. Moiseyev, Quantum theory of resonances: Calculating energies, widths and cross-sections by complex scaling, *Phys. Rep.* **302**, 211 (1998).
- [26] P. A. Belov, An estimate for the nonradiative linewidths of the quasibound electron-hole pairs in narrow quantum wells, *Semiconductors* **53**, 2049 (2019).
- [27] P. Rommel, P. Zielinski, and J. Main, Green exciton series in cuprous oxide, *Phys. Rev. B* **101**, 075208 (2020).
- [28] P. Rommel, J. Main, S. O. Krüger, and S. Scheel, Inter-series dipole transitions from yellow to green excitons in cuprous oxide, *Phys. Rev. B* **104**, 085204 (2021).
- [29] P. Belov, F. Morawetz, S. O. Krüger, N. Scheuler, P. Rommel, J. Main, H. Giessen, and S. Scheel, Energy states of excitons in finite crystals (2023), arXiv:2310.19746.
- [30] U. Fano, Effects of configuration interaction on intensities and phase shifts, *Phys. Rev.* **124**, 1866 (1961).
- [31] F. H. Stillinger and D. R. Herrick, Bound states in the continuum, *Phys. Rev. A* **11**, 446 (1975).
- [32] N. Moiseyev and J. Katriel, The Gaussian potential: Bound states in the continuum?, *Theoret. Chim. Acta* **41**, 321 (1976).
- [33] C. W. Hsu, B. Zhen, A. D. Stone, J. D. Joannopoulos, and M. Soljačić, Bound states in the continuum, *Nature Reviews Materials* **1**, 16048 (2016).
- [34] D. B. Tran Thoai, R. Zimmermann, M. Grundmann, and D. Bimberg, Image charges in semiconductor quantum wells: Effect on exciton binding energy, *Phys. Rev. B* **42**, 5906 (1990).
- [35] P. A. Belov and E. S. Khramtsov, The binding energy of excitons in narrow quantum wells, *Journal of Physics: Conference Series* **816**, 012018 (2017).
- [36] E. S. Khramtsov, P. A. Belov, P. S. Grigoryev, I. V. Ignatiev, S. Y. Verbin, Y. P. Efimov, S. A. Eliseev, V. A. Lovtcius, V. V. Petrov, and S. L. Yakovlev, Radiative decay rate of excitons in square quantum wells: Microscopic modeling and experiment, *Journal of Applied Physics* **119**, 184301 (2016).
- [37] A. U. Hazi and H. S. Taylor, Stabilization method of calculating resonance energies: Model problem, *Phys. Rev. A* **1**, 1109 (1970).
- [38] V. A. Mandelshtam, T. R. Ravuri, and H. S. Taylor, Calculation of the density of resonance states using the stabilization method, *Phys. Rev. Lett.* **70**, 1932 (1993).
- [39] V. A. Mandelshtam, H. S. Taylor, V. Ryaboy, and N. Moiseyev, Stabilization theory for computing energies and widths of resonances, *Phys. Rev. A* **50**, 2764 (1994).
- [40] D. Delande, A. Bommier, and J. C. Gay, Positive-energy spectrum of the hydrogen atom in a magnetic field, *Phys. Rev. Lett.* **66**, 141 (1991).
- [41] J. Main and G. Wunner, Ericson fluctuations in the chaotic ionization of the hydrogen atom in crossed magnetic and electric fields, *Phys. Rev. Lett.* **69**, 586 (1992).
- [42] N. Elander and E. Yarevsky, Finite-element calculations of the antiprotonic helium atom including relativistic and qed corrections, *Phys. Rev. A* **56**, 1855 (1997).
- [43] V. V. Serov, V. L. Derbov, T. A. Sergeeva, and S. I. Vinitzky, Hybrid surface-flux method for extraction of the ionization amplitude from the calculated wave function, *Phys. Rev. A* **88**, 043403 (2013).
- [44] P. Belov and R. Arkhipov, Formation of the stopped polarization pulse in a rectangular quantum well, *Micro and Nanostructures* **180**, 207607 (2023).
- [45] G. Jolicard and E. J. Austin, Influence of electron-hole plasma on Rydberg excitons in cuprous oxide, *Chem. Phys. Lett.* **121**, 106 (1985).
- [46] V. A. Mandelshtam, H. S. Taylor, V. Ryaboy, and N. Moiseyev, Stabilization theory for computing energies and widths of resonances, *Phys. Rev. A* **50**, 2764 (1994).
- [47] L. Zhang, S.-G. Zhou, J. Meng, and E.-G. Zhao, Real stabilization method for nuclear single-particle resonances, *Phys. Rev. C* **77**, 014312 (2008).
- [48] G. Bouskila, A. Landau, I. Haritan, N. Moiseyev, and D. Bhattacharya, Complex energies and transition dipoles for shape-type resonances of uracil anion from stabilization curves via Padé, *The Journal of Chemical Physics* **156**, 194101 (2022).
- [49] E. Hiyama, R. Lazauskas, and J. Carbonell, 7H ground state as a 3H+4n resonance, *Physics Letters B* **833**, 137367 (2022).
- [50] L. D. Landau and L. M. Lifshitz, *Quantum Mechanics Non-Relativistic Theory, Third Edition: Volume 3* (Butterworth-Heinemann, 1981).
- [51] N. Moiseyev, P. Certain, and F. Weinhold, Resonance properties of complex-rotated hamiltonians, *Molecular Physics* **36**, 1613 (1978).
- [52] J. Wilkes and E. A. Muljarov, Exciton effective mass enhancement in coupled quantum wells in electric and magnetic fields, *New Journal of Physics* **18**, 023032 (2016).
- [53] D. Ziemkiewicz, G. Czajkowski, K. Karpiński, and S. Zielińska-Raczyńska, Electro-optical properties of excitons in Cu<sub>2</sub>O quantum wells. II. Continuum states, *Physical Review B* **104**, 075303 (2021).
- [54] C. De Boor, ed., *A practical guide to splines* (Springer, New York; Heidelberg, 2001).

- [55] H. Bachau, E. Cormier, P. Decleva, J. E. Hansen, and F. Martín, Applications of B-splines in atomic and molecular physics, *Reports on Progress in Physics* **64**, 1815 (2001).
- [56] D. Kahaner, C. Moler, and S. Nash, *Numerical methods and software* (Prentice Hall, 1989).
- [57] E. Anderson, Z. Bai, C. Bischof, L. S. Blackford, J. Demmel, J. J. Dongarra, J. Du Croz, S. Hammarling, A. Greenbaum, A. McKenney, and D. Sorensen, *LAPACK Users' Guide (Third Ed.)* (Society for Industrial and Applied Mathematics, Philadelphia, PA, USA, 1999).
- [58] R. B. Lehoucq, D. C. Sorensen, and C. Yang, *ARPACK Users' Guide* (Society for Industrial and Applied Mathematics, 1998).